

1 Research background and Fundamentals

1.1 Radiotherapy

Since the discovery of X-rays in 1895 the radiation has been used by physicians for treating patients. In the beginning only superficial diseases could be cured, but as time and technology progressed X-ray tubes gained on voltage and allowing treatment of deeper suited tumors.

The radiation from linear accelerator was first used in medicine in 1953. Because the beam is more collimated and energies are higher than X-ray tube the cure rates improved tremendously. The next big milestone was introduction of computers in the field of radiotherapy. This led to better diagnostic tools, such as computed tomography scans (CT), magnetic resonance imaging (MRI) and positron emission tomography (PET). With those tools the location of the tumor could be much better estimated and hence the physicians could easier prescribe treatment. The potential of computers were afterwards exploited also in treatment planning with intensity modulated radiation therapy (IMRT) which, together with diagnostic tools, provides an exact dose shaping in accordance to patient specific tumors.

In 1946 it was discovered that protons could be used alongside photons for cancer treatment. Furthermore it was shown that protons have preferable depth dose profile compared to photons. First patient treatment soon followed in the early 1950's at Lawrence Berkeley Laboratory, USA. Heavier ions, such as He^{2+} , ${}^{20}\text{Ne}$ and ${}^6\text{C}$ were also used later on for treatment. In the beginning only passive beam delivery was used for treatment and in the 1990's active beam solutions were developed at Paul Scherrer Institut (PSI), Villigen (Switzerland) for protons and at GSI, Darmstadt (Germany) for carbon ions.

Both treatment modalities (photons and ions) use the same principle to eliminate cancer cells. The physical and biological mechanism behind it will be explained in detail in the following sections.

1.2 Physical and biological basics of radiotherapy

1.2.1 Interaction of radiation with matter

The interactions between photons and ions with matter are quite different, as can be seen from depth dose distributions in Figure 1.1. Photons deposit highest local dose shortly after entering

the matter (at the energies used in radiotherapy). Ions deposit most of their dose right before they stop in the Bragg Peak region. The position of the Bragg Peak depends on the energy of the ions, which is exploited in the treatment of deep seated tumors.

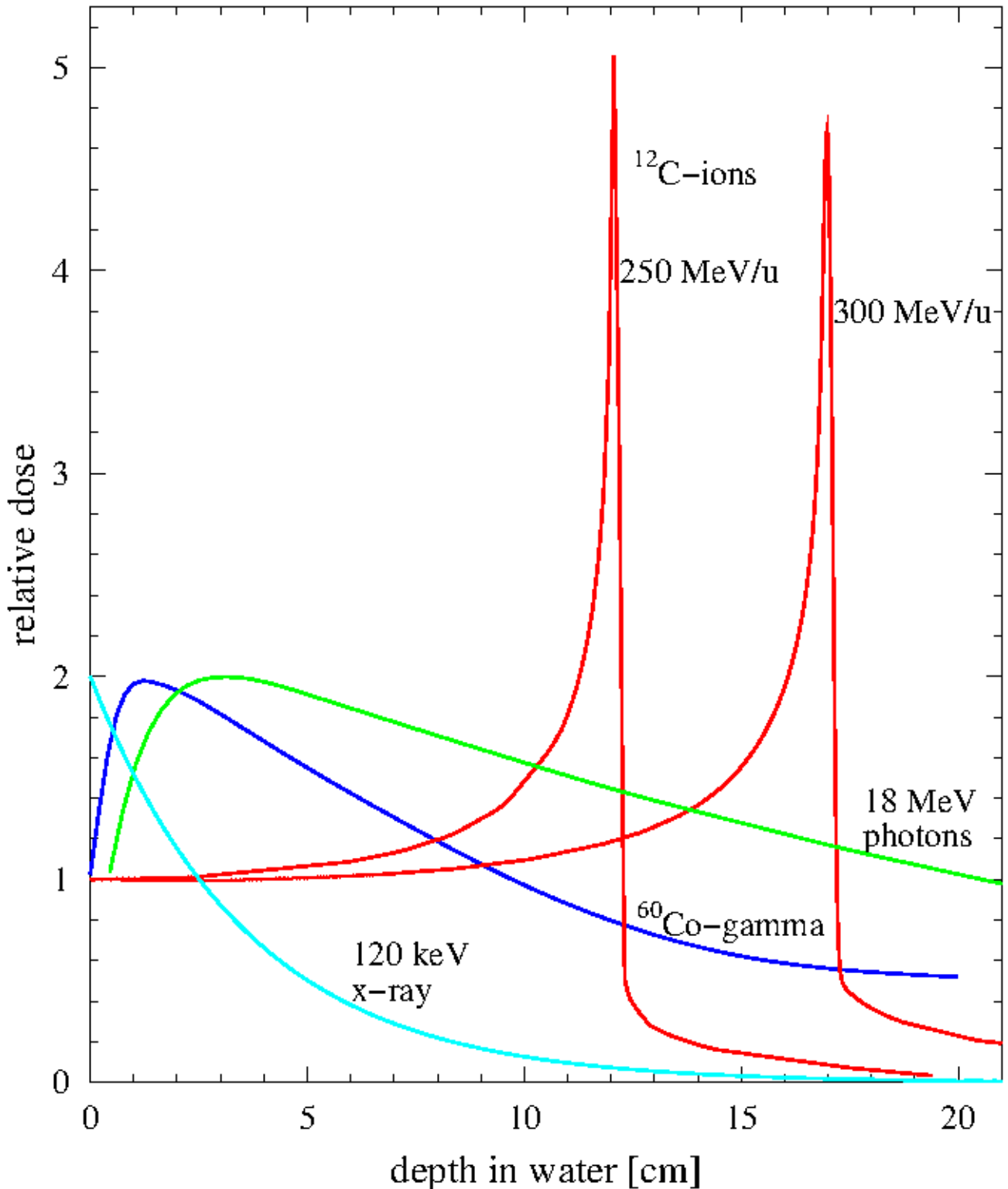


Figure 1.1: Photon and carbon ions depth dose distributions at different energies. Photons start with a build up, which is followed by an exponential decrease after. Ions deposit most of the dose at the end of the particle track, the Bragg peak. Figure taken from [Schardt et al., 2010]

1.2.2 Dose definition

Physics in radiotherapy revolves around dose, D , which is defined as the ratio of the absorbed energy dE per mass element dm [ICRU, 1993b]:

$$D = \frac{dE}{dm} \quad \left[Gy = \frac{J}{kg} \right] \quad (1.1)$$

Usually we can describe energy loss of a beam in a thin layer of material, dE/dx . Dose can be then rewritten as:

$$D = \frac{dE}{dx} \times \frac{1}{F} \times \frac{1}{\rho} \quad (1.2)$$

where F is fluence and ρ the material density.

Interaction of photons with matter

Photons mostly interact with matter in one of the following ways: coherent or Rayleigh scattering, photoelectric effect, Compton scattering and pair production. The cross section, σ , for each of these processes depends as well on the energy of the incident photons as on the atomic number of the absorber material [Lilley, 2006]. The decreasing photon intensity in matter, I , can be described as:

$$I = I_0 \cdot e^{-N\sigma x} = I_0 \cdot e^{-\mu x} \quad (1.3)$$

where I_0 stands for the initial intensity of the photons, x the depth of the material in units of length, N the atomic density of the material and μ is the attenuation coefficient. The cross section, *sigma* is the sum of all possible interaction processes.

$$\sigma = \sigma_{rayleigh} + \sigma_{photoelectric} + Z\sigma_{compton} + \sigma_{pairproduction} \quad (1.4)$$

The energy range of photons used in radiotherapy is between 100 keV and 25 MeV. The dominating process in this energy range is Compton scattering [Alpen, 1998]. The electrons resulting from Compton interaction scatter mostly in a forward direction. Therefore a maximum of the depth-dose profile occurs when electrons stop at a certain depth, the mean electron range. After this build up the dose deposition decreases exponentially (see Figure 1.1 and Equation 1.3).

Interaction of ions with matter

Ions can interact with matter either with elastic columb scattering from target nuclei (nuclear stopping) or with inelastic collision with target electorns (electronic stopping). At the ion energies used in radiotherapy, which are less then 500MeV/u, the electronic stoping is the dominated interaction. This results in ionization and excitation of the atoms in target.

The mean rate of ions energy loss in matter is described by the Bethe-Bloch formula [Bethe, 1930, Bloch, 1933]. Since we are interested in low ion energies, we can make the following approximation:

$$-\left\langle \frac{dE}{dx} \right\rangle = \frac{4\pi N_e z_{eff}^2}{m_e v^2} \left(\frac{e^2}{4\pi\epsilon_0} \right)^2 \left[\ln \left(\frac{2m_e v^2}{I} \right) + \text{correction} \right] \quad (1.5)$$

here N_e is the materials electron density, e and m_e are the charge and mass of an electron, ϵ_0 the electrical field constant and I the mean excitation energy of the absorber material. Barkas formula [Barkas, 1963] can be used for the approximation of the effective projectile charge z_{eff} :

$$z_{eff} = z \left(1 - e^{-125\beta z^{2/3}} \right) \quad (1.6)$$

where β is the projectile speed in units of c .

The energy loss of ions is proportional to z_{eff} and inversely proportional to v^2 . The shape of the curve in Figure 1.1 can now be understood. Ions enter the matter with a high velocity, resulting in a small energy deposition. Their velocity gradually decreases, which in turn increases the energy deposition. The maximum of the energy loss is called Bragg peak or particle range.

Lateral scattering and range straggling of ions

As mentioned in section 1.2.2 ions interact mostly via electronic stopping at energies used in radiotherapy. However, nuclear stopping still occurs and it is the main reason for lateral scattering. The angular spread of ions is dependent on the mass of the target nuclei and on the momentum of the indecent ions [Molière, 1948]. The lateral scattering is proportional to mass of the target nuclei and inversely proportional on the momentum of indecent ions. Carbon ions have thus less lateral scatter then protons. Experiments have shown that carbon ions have three times smaller angular spread compared to protons at the same range in water (15.6 cm, 150 MeV/u protons and 285 MeV/u ^{12}C ions) [Schardt et al., 2010].

Statistical fluctuations of specific electronic stopping events cause range straggling of ions. If the number of collisions is high or the material is thick enoguh these fluctuations can be

approximated by a Gaussian probability distribution [Bohr, 1940, Ahlen, 1980]. The straggling width σ_R is proportional to:

$$\sigma_R \propto R/\sqrt{M} \quad (1.7)$$

where R is the mean range of ions and M the ion mass. Thus, the heavier the ion is, the less range straggling it has. Carbon ions have 3.5 smaller range straggling when compared to protons [Schardt et al., 2010].

Nuclear fragmentation

When transversing through matter ions (except protons) can be fragmented into ions with lower Z. The lower Z fragments travel in the same direction as projectile ions and have a significant contribution to the dose deposited (see Figure 1.2). It is essential that these fragments are included in the treatment planning, so that the accurate dose can be assessed.

After colliding with target projectile fragments enter an excited state. De-excitation occurs through emission of nucleons, nucleon clusters and photons. Two of the possible fragments of projectile ^{12}C ions are isotopes ^{11}C and ^{10}C , which are both β^+ emitters [Kraft, 2000]. The resulting positron is annihilated with electrons in matter, resulting in two photons traveling in opposite directions. This can be used in PET (Positron Emission Tomography) without exposing patient to additional radiation..

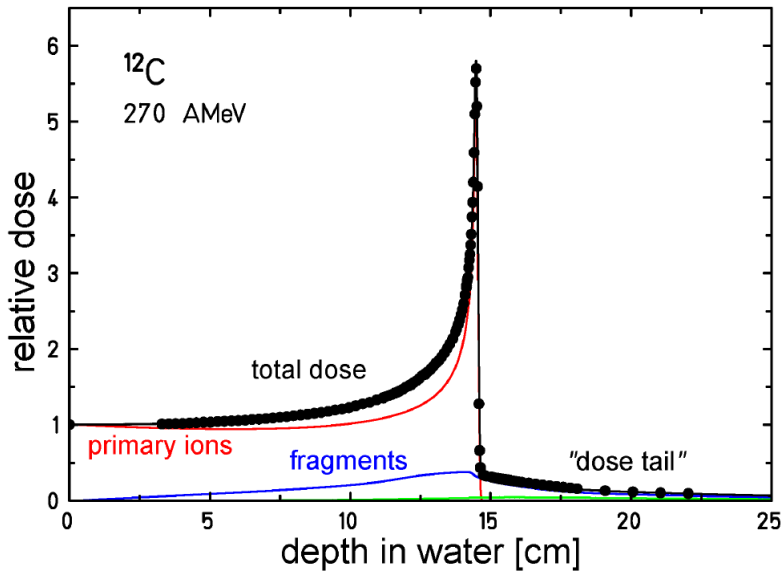


Figure 1.2: Impact of fragmentation on a depth dose distribution of carbon ions. Main contribution to the overall deposited dose (black line) comes from the primary ions (red line). The produced fragments (blue line) have a smaller impact, but non-negligible especially in the dose tail behind the Bragg peak. Figure taken from [Groezinger, 2004]

As mentioned in section 1.2.2 ions used in radiotherapy lose most of their energy via inelastic Coulomb scattering on target electrons. Such electrons can be libirated from target atoms and are called secondary electrons, also δ -electrons. δ -electrons also travel throguh matter, further scattering and may even cause secondary ionization of the target atoms. When δ -electrons energies are larger than >50 eV, ionization becomes dominant process, which produces a large number of additional electrons [Kraft, 2000, Schardt et al., 2010].

The radial dose profile and track diameter is defined by the energy spectrum of the δ -electrons. Most of the δ -electorns are concentrated around the projectile ions path, since they receive small energy transfers or are scattered in the direction of indicent ions. Different models [?], Monte Carlo simulations [?] predict radial dose fall-off approximately with $1/r^2$ for radial distances r . Varma et. al. have confirmed this experimentaly [Varma et al., 1977]. The maximum radial distance r_{max} is defined by the most energetic δ -electrons, which are related to energy, E , of the projectile ions [Kiefer and Straaten, 1986].

$$r_{max} = E^{1.7} \quad (1.8)$$

Following equation 1.5, E is corelated to Z^2 and $1/\beta^2$, which means track structure is highly dependent on the projectile ion species and energy. This is well demonstrated on Figure 1.3: Carbon ions have much more dense ionization structure compared to protons [?]. δ -electrons have low energies, and thus the r is on nanometer scale. As the energy of projectile ions decreases, their stopping power increases and causes significantly larger number of δ -electorns. The energy deposited by δ -electrons in medium is described using the Linear Energy Transfer (LET), which is closely related to dE/dx . Fast ions, with little ionization, have thus small LET, while slow ions, with large ionization, have a high LET.

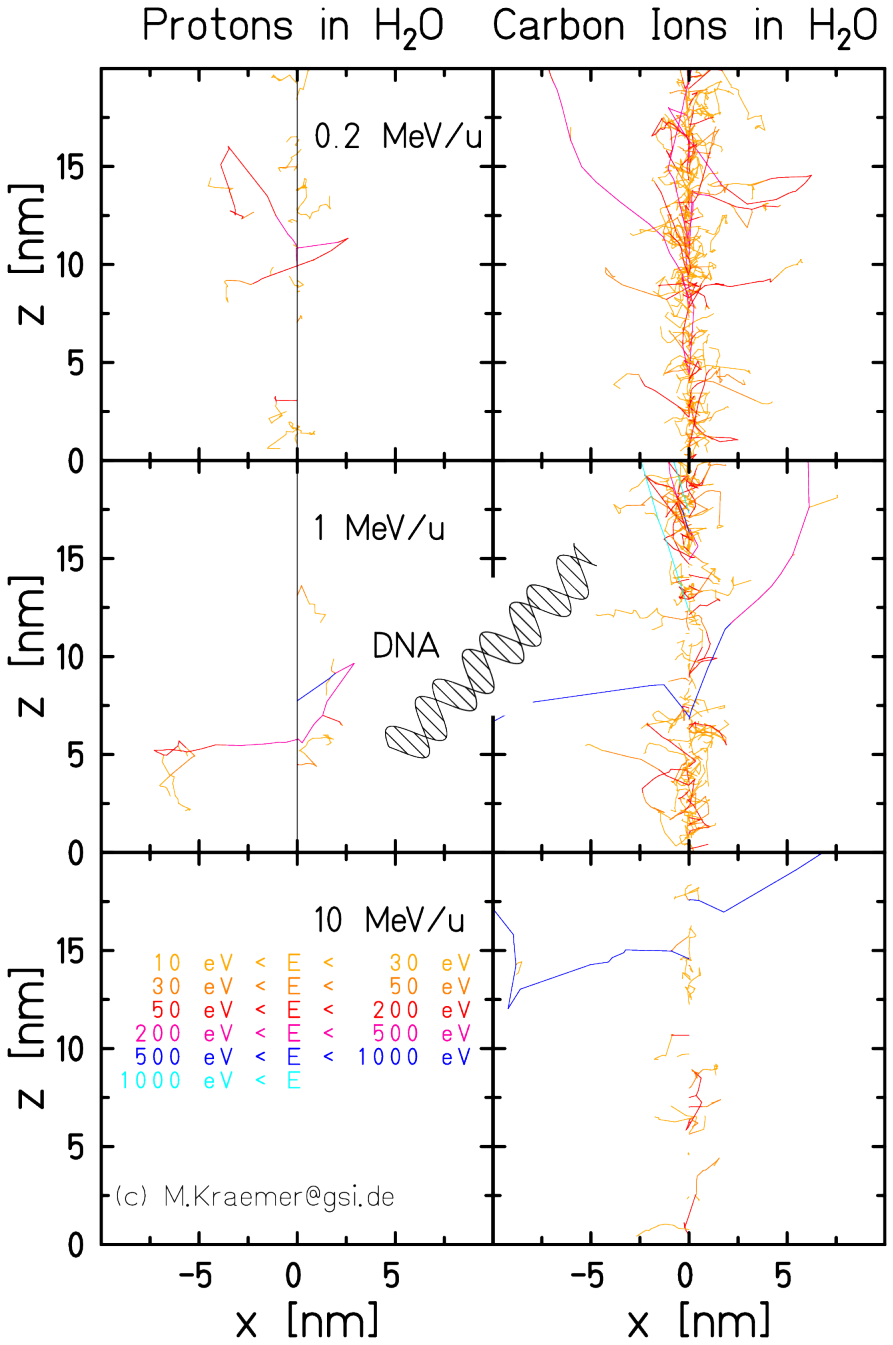


Figure 1.3: Track structure of ions in water at different energies. The distribution of δ -electrons is highly dependent on ion species and their energy. A molecule of DNA is displayed for size comparison. Figure courtesy of Michael Krämer.

1.2.3 Radiobiology

The aim of radiotherapy is to kill tumor cells and prevent further growth, while sparing healthy tissue. Ionizing radiation (photons and ions) causes damage throughout the cell. However the most susceptible part to radiation is the carrier of genetic information, the deoxyribonucleic acid (DNA), located in the cell nucleus [Munro, 1970]. Radiation can destroy DNA in two

ways - directly or indirectly. Ionization and consequent destruction of DNA molecular bonds via radiation is a direct effect (see Figure 1.4b) and is typical for high-LET radiation. On the other hand, an indirect effect is when radiation hydrolyses water around DNA and produce highly reactive hydroxyl-radicals, OH (see Figure 1.4a). Eventhough their lifetime is short, it's enough to cause severe damage to DNA. The formation of OH is typical for low-LET radiation, like photons. The two processes, direct and indirect, are not excluding and can damage DNA in parallel.

Damage to DNA can result in either single strand breaks (SSB) or double strand breaks (DSB) as shown in Figure 1.4b). When one of the double strands in the DNA helix is destroyed (SSB), it can be usually easily repaired by cell repair-mechanisms, since the complementary base is intact. If bases on both stands are destroyed (DSB) the DNA damage is much more complex and can lead to the breakage of the chromatin. The cell repair-mechanisms can handle DSB as well, albeit not that efficient as SSB. However if there are clustered DSBs, the damage is usually too severe for repair-mechanisms to undo it. The changes in damaged DNA can lead to carcinogenesis or cell death. The aim of radiotherapy is to cause apoptosis - a controlled self-inactivation of the cell due to DNA damage. Beside apoptosis, there is necrosis, an uncontrolled cell death. Cell necrosis often cause response from the immune system, leading to inflammation, which radiotherapy tends to avoid.

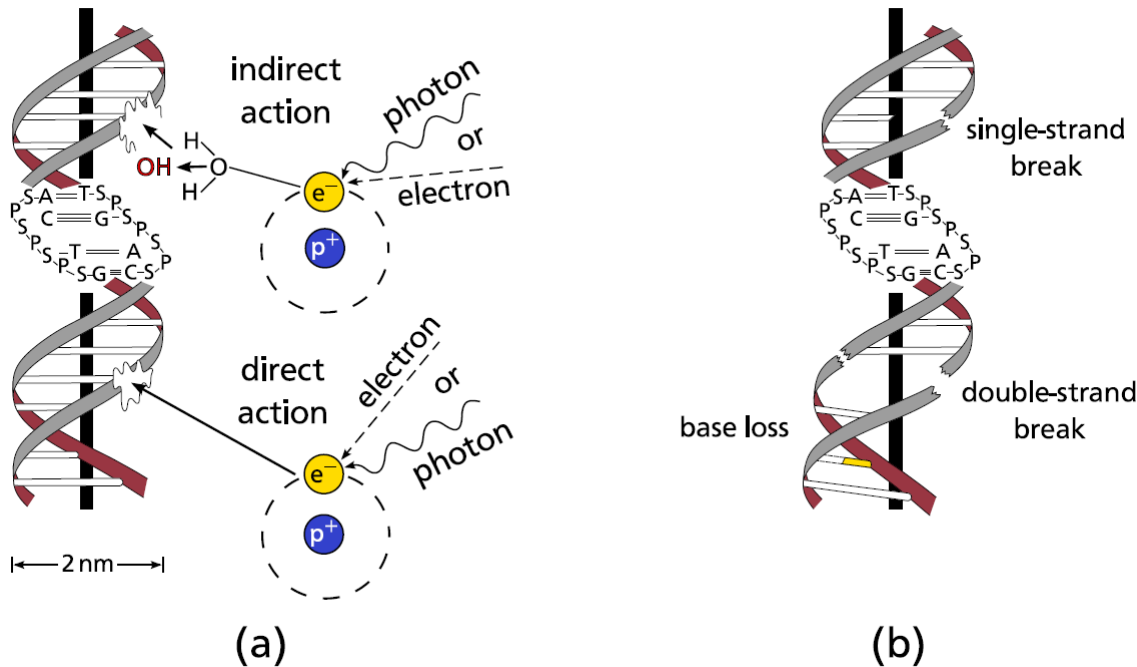


Figure 1.4: Types of DNA damage caused by radiadtion. (a) Indirect damage occurs, when radiation forms free radicals hydroxyl radicals (OH), which can damage DNA. (b) Direct effects of radiation can cause single or double-strand breaks. Figure taken from [Richter, 2012]

Relative Biological Effectiveness

Figure 1.3 shows the size of DNA molecule in comparison with proton and carbon ion distribution of δ -electrons around their track. Clustered DSB occur around ions Bragg peak due to the large ionization densities. As mentioned this poses a too large of a difficulty for cell repair-mechanisms, leading to cell death. The large ionization density is typical for ions and is one of the main advantages over photons in radiotherapeutic sense. Since most of the research about cell response to radiation was done for photons, the biological effect of ions is usually described relative to a reference photon response. Relative biological effectiveness (RBE) is therefore defined as the ratio of the reference photon dose to the dose level of a specific ion radiation at the same biological effect (isoeffect):

$$RBE = \left. \frac{D_{photon}^{ref}}{D_{ion}} \right|_{isoeffect} \quad (1.9)$$

It is important to note at this point that RBE values are valid only for the same effect, the same biological endpoint and the same reference radiation. The most interesting biological endpoint in radiotherapy is cell survival and side effects. RBE values are usually obtained from the cell survival curves (see Fig. ??). Cell survival curves, S , are commonly described by an exponential linear-quadratic model:

$$S(D) = \exp(-\alpha D - \beta D^2) \quad (1.10)$$

characteristic of a tissue (cell) type is written in the α/β ratio, namely the tissue capacity to repair radiation damage. A small α/β ratio means cell is radioresistant (high repair capacity) and vice versa. As seen in Figure 1.5 and Eq. 1.10 RBE values are dependent on dose level. Hence in ion radiotherapy, beside the physical absorbed dose, a photo-equivalent or biological dose incorporating the RBE also plays an important role. The unit for biological dose is Gy (RBE) [ICRU, 2007].

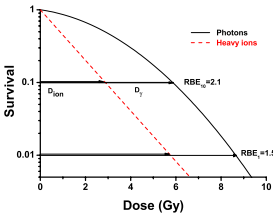


Figure 1.5: Typical cell survival curve for photons (black solid line) and heavy ions (red dashed line). Photon line shows typical shouldered form, described by linear-quadratic model. Heavy ions show a much steeper decrease with dose. The RBE value can be calculated by looking at the points at the same survival value - same biological effect. Figure taken from [Schardt et al., 2010]

Beside dose level, RBE among other depends also on the LET, the particle species and the tissue type [Kraft, 2000]. Therefore RBE modeling is a very complex issue. At GSI RBE is calculated using *local effect model* (LEM) developed by Scholz et al [Scholz and Kraft, 1994]. The main assumption in LEM model is that biological effects are independent on the radiation type. The difference between different radiation types comes from the dose deposition in a small volume in the cell nucleus. At the same total dose, photons have a homogeneous dose distribution over a cell nucleus, while ions have a highly localized dose distribution (around ion track). Next assumption of the LEM is that the photon response is the same at these high local doses. With this assumption ion dose response can be predicted, by comparing photon response at the high local dose level. LEM has received several revisions [Elsaesser and Scholz, 2006, Elsaesser and Scholz, 2007, Elsaesser et al., 2009] and experimental verifications [Mitaroff et al., 1998, Krämer and Scholz, 2000, Krämer et al., 2003], making it valid for clinical use. RBE for carbon ions ranges from 1 in the entrance channel, to a value around 5 at the Bragg peak [Kraft, 2000]. The highest RBE for carbon ions is right around Bragg peak, which gives carbon ions a great advantage, since there is an increased biological effectiveness at target tissue compared to the normal tissue in the entrance channel. In proton therapy a constant RBE value of 1.1 across the treatment field is used [Paganetti et al., 2002].

1.2.4 Application technique

Introduction

Photon therapy

Ion therapy

In order to ion therapy be successful, ions must be accelerated to appropriate energies (several hundred MeV/u), the beam must be transported to target area and guided onto the target with necessary accuracy (around 1 mm). This requires very complex delivery systems and is one of the reason ion therapy is not as common as photon one.

Two types of particle accelerators are used in ion therapy - cyclotrons and synchrotrons. **Cyclotrons** can be built in a compact design and offer a continuous beam with stable intensities. Particle energy, however, can not be regulated and therefore passive energy degraders are needed. Active energy variation is possible with **synchrotrons**, where a linear accelerator is used to inject ions into the synchrotron and then the beam is regulated with ion optics. Synchrotrons are used in all heavy ion therapy centers, while cyclotrons are most commonly used in proton therapy.

Each tumor has a unique shape, size and position in patient. Therefore a single Bragg peak would not provide adequate dose and a beam shaping has to be employed. Two beam shaping systems can be used - passive and active beam shaping. In the next two sections both will be explained, with focus on active beam shaping, which was used later in simulations.

Passive beam shaping

The general idea of passive beam shaping is to transform a beam into the shape of the tumor. This is done in several steps as schematically shown in Fig. 1.6. Firstly, the beam is broadened using a scattering device (passive double scattering systems or magnetic wobbler) in order to obtain a broad, flat profile. In the next step, the beam is spread out over the required energy range with a range modulator. Usually range modulator are a rotating wheels of various thickness or a ridge filter [Chu et al., 1993]. A single Bragg Peak is thus spread out into so-called *spread-out Bragg peak (SOBP)*, which is moved to the required depth using a range shifter. The final two devices in beam's path are built for each patient individually. Collimator shapes beam in a lateral direction, while compensator adjusts SOBP to the distal edge of the tumor. However, compensator cannot adjust dose in the proximal edge of the tumor, resulting in an access dose to the healthy tissue (hatched area in Fig. 1.6).

Passive beam shaping offers more robust and faster treatment delivery in contrast to active beam shaping. However, it lacks tumor conformity, dose cannot be modulated and each patient needs individually tailored devices for each beam used in treatment. Furthermore beam travels through some material, exposing patient to additional dose due to fragmentation.

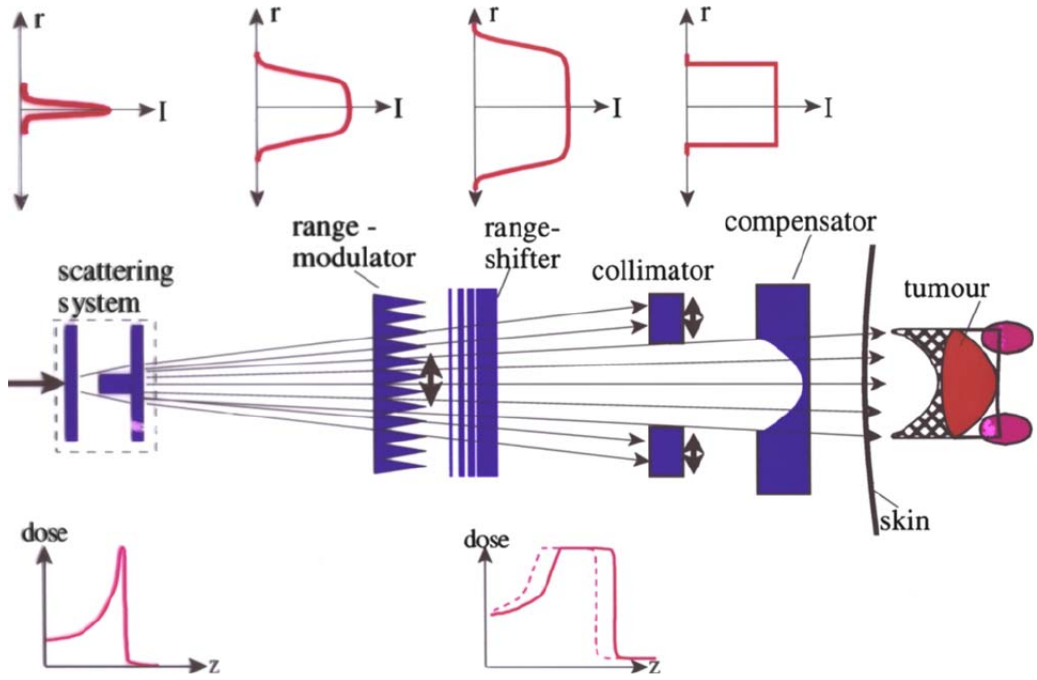


Figure 1.6: Schematic presentation of a passive beam shaping. A scattering system is used to broaden the beam. afterwards a range modulator spreads out Bragg Peak to the required energy range. The spread out Bragg peak is then shifted to a fixed range with a range modulator. Finally patient specific collimator and conformator serve for lateral and longitudinal conformity, respectively. The proximal edge of the tumor cannot be shaped, as shown with hatched area. Figure taken from [?].

Acitve beam shaping

In contrast to passive beam shaping, active beam shaping works by dividing tumor into small points, which are then irradiated using a thin pencil beam. Tumor is first segmented into iso-energy slices (IES) and each of IES is then covered with 2 dimensional grid. A thin pencil beam travels from point to point on this grid, irradiating each point with designated dose. This technique allows irradiation of arbitrary shape, without introducing additional, patient specific hardware. The lack of additional material in front of the patient also means less dose due to lesser neutron flux. Furthermore with the option to modulate dose in each point, dose in tumor is very conformal with less dose to healthy tissue.

There are differences in specifics of active beam shaping, so the GSI system of three-dimensional scanning system will be presented here [Haberer et al., 1993, Kraft, 2000, Schardt et al., 2010] and a schematic presentation in Fig. 1.7 and Fig. 1.8. Synchrotron provides a thin pencil beam of ^{12}C ions with selected energy. The energy defines the position of the Bragg peak in depth. Fig. 1.8b shows how are Bragg peaks stacked in depth to cover longitudinal extension of the tumor. IES is covered with 2 dimensional grid of target points

(raster points). The thin pencil beam travels continuously over raster points. It is guided by two magnetic deflection units. In treatment planning each raster point is designated a specific dose. During treatment the beam stays on each raster point until intensity monitoring system measures the designated dose. Then it moves to the next raster point. When the whole IES is irradiated, the treatment halts until next beam energy for next IES comes from accelerator.

Fig. 1.8a displays how dose homogeneity in target is achieved. In typical configuration beam's full width half maximum is three times the lateral raster spacing. Such configuration offers robustness for uncertainties of the beam spots. There also should be enough overlap between individual Bragg peaks. However, there should not be too many of IES, since the changing of the beam energy takes most of the time and hence prolongs the treatment. So instead of using high number of IES, Bragg peaks are broadened in longitudinal direction by using ripple filter (RiFi) - device similar to ridge filters used in passive beam shaping.

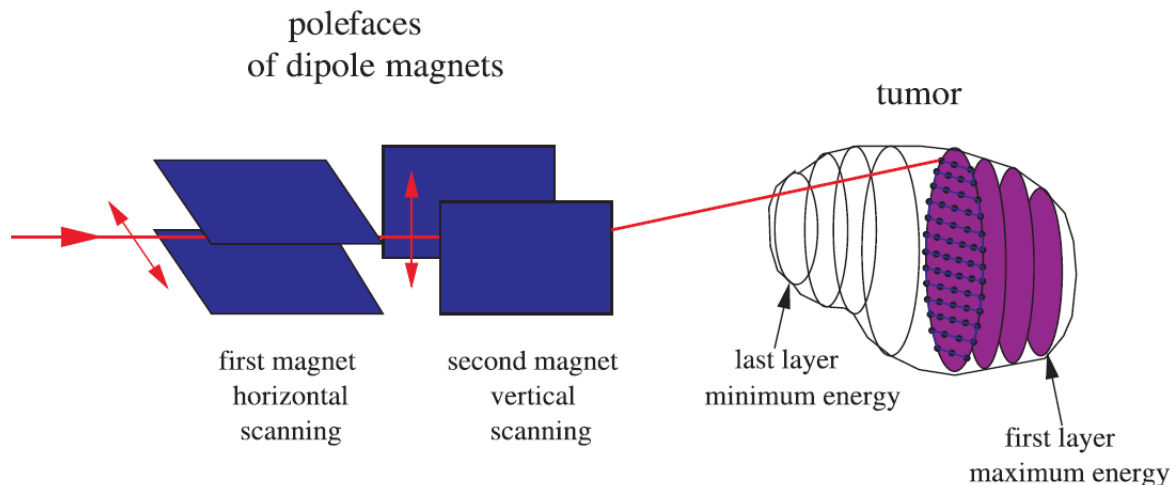


Figure 1.7: Schematics of GSI's active beam shaping. Tumor is divided into isoenergy slices, which are further overlayed with a 2 dimensional grid. Longitudinal direction (in beam's eye view) is varied with particle energy from accelerator, while lateral is via a magnetic scanning system. Figure taken from REFERENCE!

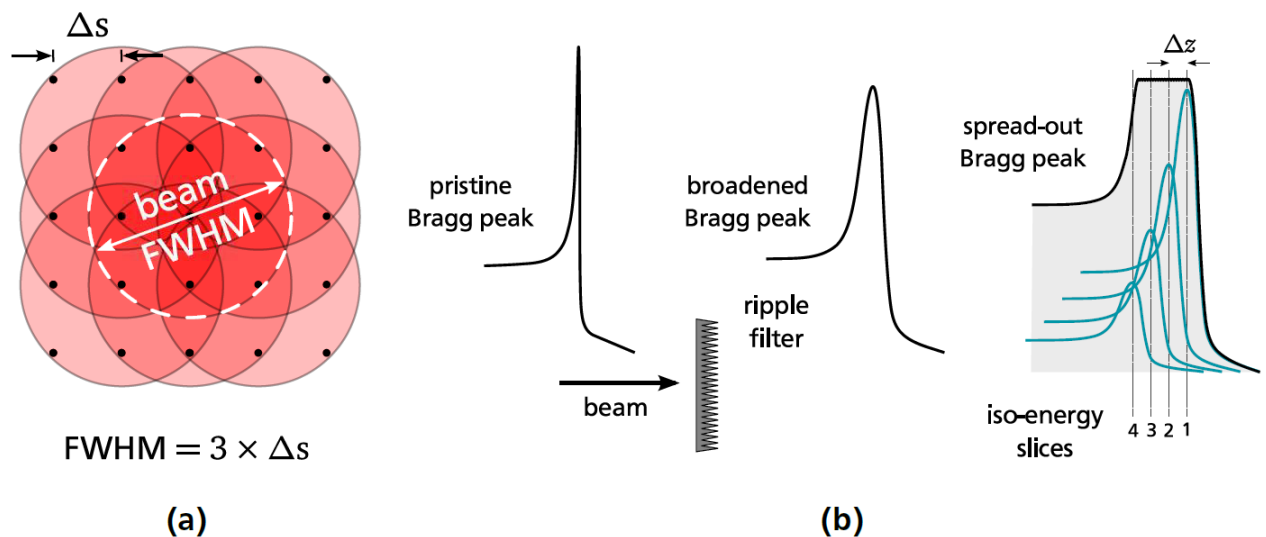


Figure 1.8: Schematic presentation of how target dose homogeneity is achieved at active beam shaping. a) To provide sufficient homogeneity in lateral direction (in beam's eye view) full width half maximum of beam is three times the spacing between raster points. b) Bragg peaks are broadened in depth with a ripple filter and then stack to provide longitudinal dose homogeneity. Figure taken from [Richter, 2012]

1.2.5 Motion in radiotherapy

Introduction

Motion types

Motion types, is's extent and origin is a vast topic. A brief introduction will be given here, for an in-depth explanation reader is pointed to review by Langen and Jones [Langen and Jones, 2001]. There are three main types of motion: patient positioning, inter- and intra-fractional motion. All three motion types are shown in Fig. 1.9.

Patient motion is difference in patient position between image acquisition (e.g. CT) used for treatment planning and actual delivery. Patient motion introduces changes in tumor shape and tumor position. To overcome patient position uncertainties, patient immobilization and dedicated protocols are used.

Interfractional motion happens between two treatment sessions (fractions) and results in anatomical changes in a patient. It has a time scale of hours and days. For lung cancer patients, tumor shrinkage and lung density change occur between fractions MORI2009. Also changes in breathing pattern can impact treatment delivery. While the breathing motion trajectory has a good reproducibilty, the tumor baseline drifts significantly [Sonke et al., 2008]. Repeated imaging and replanning reduces the impact of the interfractional motion.

Intrafractional motion usually stands for respiration and heart beat. It has a time scale from seconds to minutes. In this thesis we will focus on respiratory motion. Respiratory motion varies from patient to patient and it is responsible for tumor motion from a mm range to a couple of cm. Tumor size and T-staging are also correlated to tumor motion [Liu et al., 2007]. The respiratory-induced motion is largest in superior-inferior (SI) direction rather than in the anterior-posterior (AP) or left-right (LR) directions.

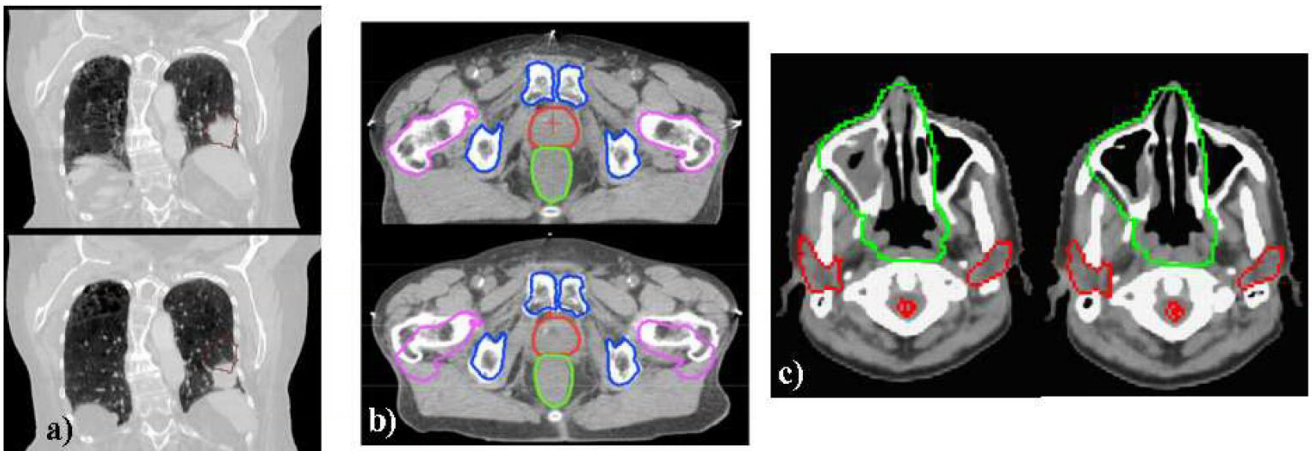


Figure 1.9: Examples of the three major motion categories. On the left side (a) a lung tumor is displayed, which moves due to the respiration of the patient (intrafractional motion). Interfractional position changes are exemplary shown in the middle (b), where two CT scans of a prostate patient are compared. Density variations between two CT scans are shown in (c). Figure taken from [?]

Motion mitigation techniques

While all three motion types have to be addressed in treatment planning, special focus will be given on the intrafractional motion mitigation. Photon radiotherapy or particle radiotherapy with passive beam shaping use larger safety margins to encompass the whole tumor motion as explained in section 1.2.6. However, larger safety margins are not enough to mitigate motion when active beam shaping is used. The beam delivery sequence and target motion interfere with one another, resulting in over- and underdosages in patients. Effect is called interplay and it has been thoroughly reviewed elsewhere [Phillips et al., 1992, Bert et al., 2008]. The effect of interplay depends on many factors, such as motion amplitude, beam direction, starting breathing phase etc. Three main techniques are currently established as mitigation to interplay: rescanning, gating and beam tracking. Several other techniques exist to reduce the effect of tumor motion, such as abdominal pressure, jet ventilation, apneic oxygenation etc., but will not be described here, since they are far from the topic of this thesis.

Rescanning or repainting, is a technique that uses advantage of statistical averaging of different interplay patterns [Phillips et al., 1992]. Instead of applying the whole dose D at once, the target is scanned N times, each time irradiated with D/N . The result is a Gaussian distribution of D around the D with no interplay (static case), as shown in Fig. 1.10. With more rescans (larger N), better dose homogeneity is achieved, because variance is proportional to $1/N$. Technically the method is the easiest to implement of the three mentioned, since no real-time motion monitoring is necessary. However, it introduces additional dosage to normal tissue. Rescanning has not yet been implemented clinically, but should be in the near future in several centers worldwide

[Furukawa et al., 2007, Zenklusen et al., 2010].

Gating applies irradiation only in a selected part of the breathing cycle in a so-called gating window (GW) [Minohara et al., 2000, Lu et al., 2006]. Usually exhale position is used as the center of the GW, as highlighted in Fig. 1.11. Motion monitoring signal is used to control beam extraction. While there is no additional normal tissue irradiation, the treatment time is prolonged due to the frequent beam interruptions as shown in Fig. 1.11. Conventional radiotherapy and passive beam shaping can also use advantage of gating to reduce the effects of motion on treatment delivery.

Beam tracking is a method, where the tumor is followed by beam throughout different motion phases in real time. Similar to gating, beam tracking is not limited to active beam shaping. It was even proposed originally for photons [Keall et al., 2001] and later implemented clinically in x-ray radiosurgery in the robotic Cyberknife Synchrony system (Accuray Inc., Sunnyvale, Ca., USA) [Brown et al., 2007, Kilby et al., 2010]. Regardless of radiation type, fast beam delivery system is necessary for beam tracking. In contrast to photon radiotherapy, beam tracking with particles need to pay special consideration to longitudinal changes. At GSI beam tracking system has been implemented. The solution for longitudinal changes was carried out by two polymethyl methacrylate (PMMA) wedges close to the target, that are operated via linear stepmotor [Saito et al., 2009], as shown in Fig. 1.12. Linear stepmotor can change the relative distance between the wedges and therefore introducing more or less material that beam travels and consequently changes beam energy (range). The beam tracking system at GSI was able to achieve high precision [Bert and Rietzel, 2007, ?, Saito et al., 2009], however, clinical implementation is not yet feasible, since internal motion monitoring that includes range change information in real-time is not fast enough.

The three motion mitigation techniques mentioned are not exclusive and can be used in parallel. Furukawa et al. made a study on a combination between rescaning and gating [Furukawa et al., 2007] and Water et al. presented a combination between rescanning and tracking [van de Water et al., 2009].

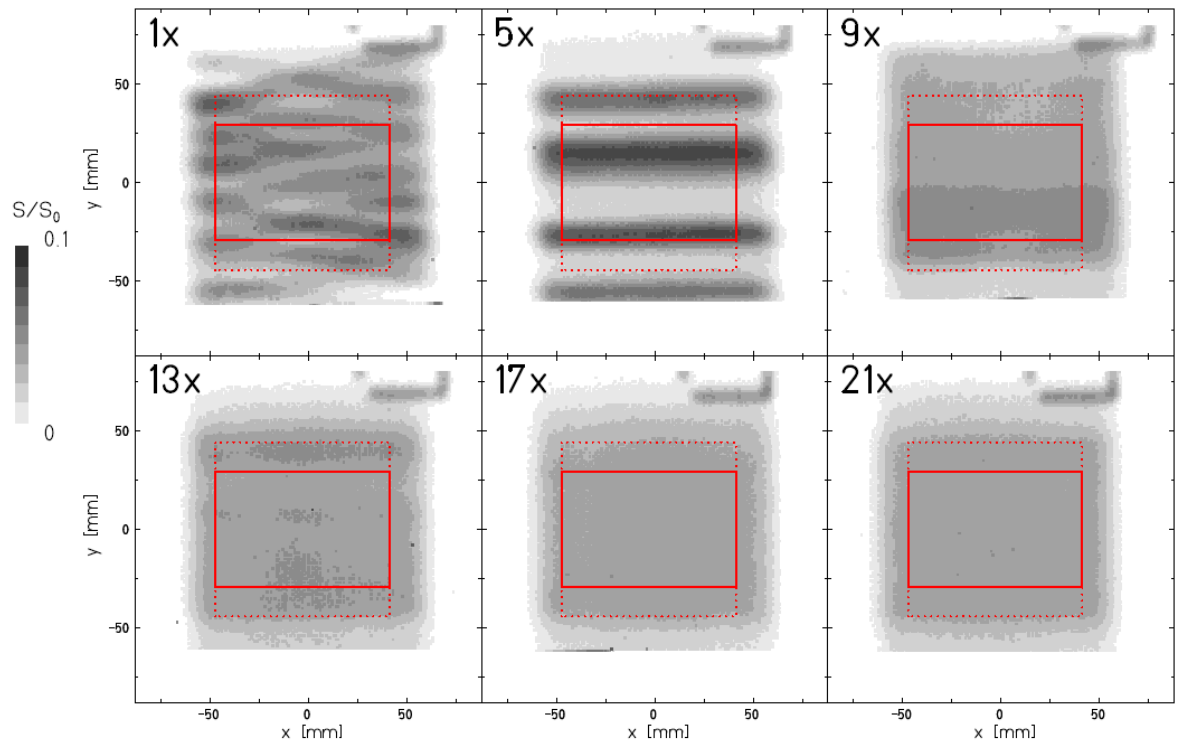


Figure 1.10: Film irradiation with rescanning. With statistical averaging of multiple interplay patterns dose in the target (solid red square) becomes homogeneous. Figure taken from [?].

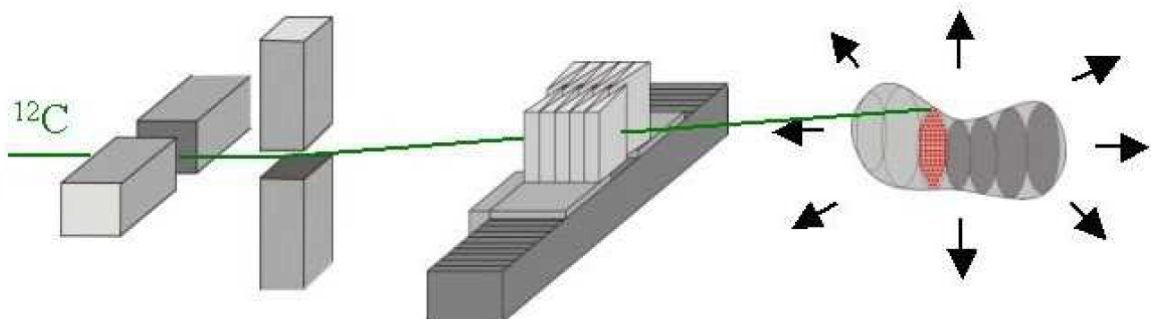


Figure 1.12: Schematic presentation of GSI's beam tracking system. Two PMMA wedges, mounted on linear stepmotor, can change the energy of the beam traveling through. The changes in lateral direction are The lateral deflection is achieved via dipole scanner magnets. For the longitudinal adaptation two PMMA wedges are mounted on step motors, enabling to change the depth the particle beam has to traverse. Figure taken from [Groezinger, 2004]

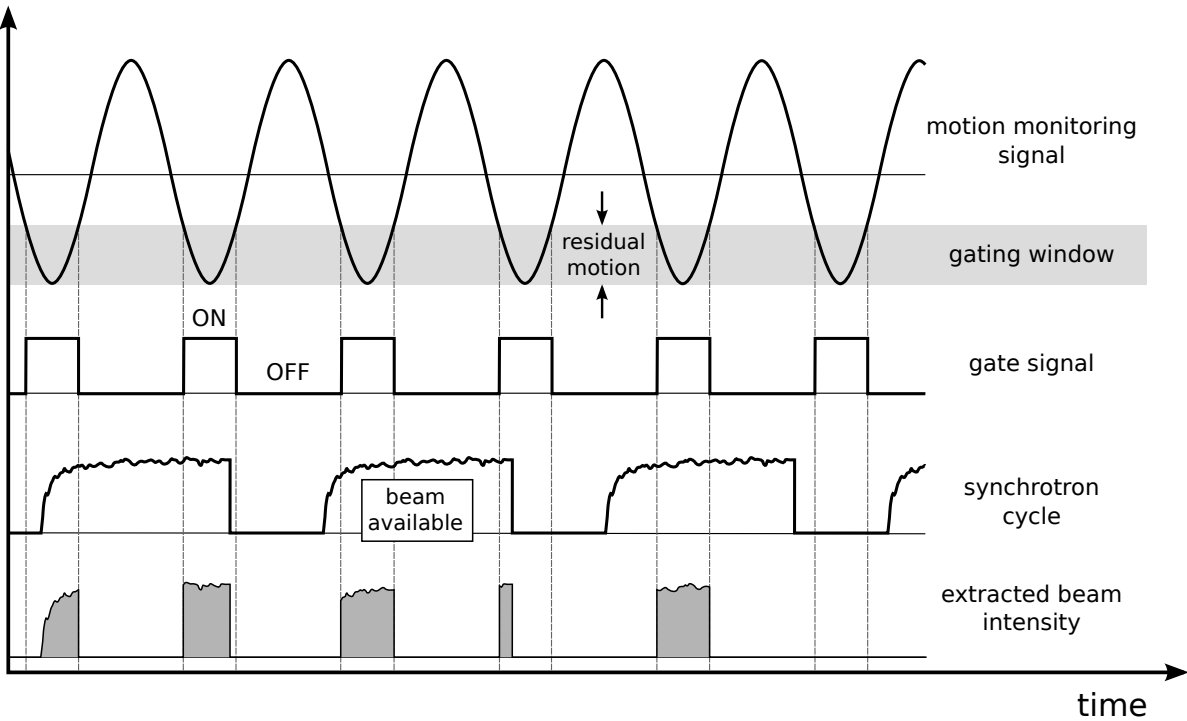


Figure 1.11: Gating delivery with a synchrotron accelerator. The irradiation is only possible, when the gate signal is active and the beam is available. The gate signal depends on gating window and motion monitoring signal.

1.2.6 Treatment planning

The task of treatment planning is to determine machine parameters in order to deliver prescribed dose to the target, while not violating maximum allowed dose to critical organs, also known as organs at risk (OARs) [Richter, 2012]. Treatment planning thus revolves around dose optimization process and it is highly dependent on delivery type used for treatment. The basis of treatment planning is computed tomography (CT), where delineation of target volume and OARs is done by physician. Additional imaging, such as magnetic resonance (MRI) or positron emission tomography (PET), is often used as a supplement to CT for even better delineation. In the following sections target definition will be explained, as well as the basics of intensity modulated photon treatment (IMPT) and scanned ion beam treatment planning. Later will be further expanded into dose calculation for moving targets.

Target definition

The definition of target volume is crucial, since it has to cover the whole tumor, prevent further tumor spreading, while at the same time it should not be too big to spare normal tissue. The International Commission on Radiation Units (ICRU) recommends the following definitions

for volumes used in treatment planning, which will also be used in this work, see Fig. ?? [ICRU, 1993a, ICRU, 1999].

Gross Tumor volume: *The GTV is the gross palpable or visible/demonstrable extent and location of malignant growth.*

Clinical Target Volume: *The CTV is a tissue volume that contains a demonstrable GTV and/or subclinical microscopic malignant disease, which has to be eliminated. This volume thus has to be treated adequately in order to achieve the aim of therapy, cure or palliation.*

Planning Target Volume: *The PTV is a geometrical concept, and it is defined to select an appropriate beam size and beam arrangements, taking into consideration the net effect of all the possible geometrical variations, in order to ensure that the prescribed dose is actually absorbed in the CTV.*

Internal Target Volume: *This is the margin that must be added to the CTV to compensate for expected physio-logical movements and variations in size, shape, and position of the CTV during therapy.*

Organs at risk: *Organs at risk (OAR) are normal tissues whose radiation sensitivity may significantly influence treatment planning and/or prescribed dose.*

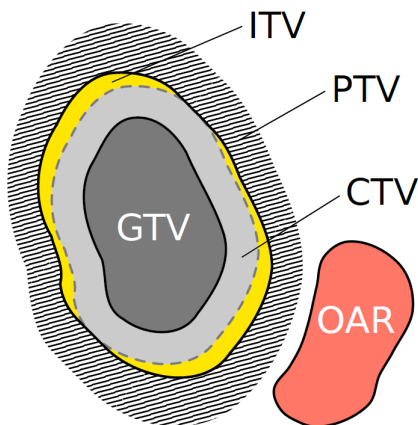


Figure 1.13: ICRU treatment planning volumes definitions. Figure taken from [Richter, 2012]

Further recommendations by ICRU state, that 100 % of the PTV volume should receive between 95 % and 107 % of the planned dose [ICRU, 1993a].

Treatment planning for scanned ion beams

Treatment planning system (TPS) for active shaping ion beams has to incorporate active beam delivery system and the beam interactions with the tissue. Furthermore, for ions heavier than

protons the biological effectiveness must also be considered, which add additional complexity to the TPS. A TPS for beam scanning was developed at GSI, called TRiP98. The basic concepts of TRiP98 will be presented here, further reading can be found elsewhere [Krämer et al., 2000, Krämer and Scholz, 2000].

TRiP98 divides PTV into energy slices, which are further divided into raster points in a defined order, that the beam will follow. In the optimization step, using least square minimization algorithm TRiP98 defines particle number for each raster point, so that the optimal target dose is achieved. Dose can either be physical or biological, using LEM biological effectiveness 1.2.3. Physical characteristic of the beam include lateral scattering as proposed by Molière [Molière, 1948] and nuclear fragmentation that yield secondary particles. The patient specific geometry and tissue inhomogeneities are accounted for using a transformation from CT HU to water-equivalent path length (WEPL) [Geiss et al., 1999, Jäkel et al., 2001, Rietzel et al., 2007].

4D Treatment planning at GSI

As mentioned in section 1.2.5 tumor motion can cause severe deficiency in treatment plan. To assess does deficiency and to overcome them, using different motion mitigation techniques, TRiP98 was expanded to be able to calculate time-resolved (4D) treatment plans. The new software was named TRiP4D and a very detailed description is given by Richter et al [Richter et al., 2013].

A static CT is not sufficient for 4D treatment planning. A time-resolved CT scans (4DCT) therefore have to be used. 4DCT consist of several quasi-stationary sections, called motion phases. Data is recorded in each slice throughout the whole motion and is then sorted to appropriate motion phases, according to motion signal [Rietzel et al., 2005].

Beside a 4DCT a vital part of 4D treatment planning is the **image registration**. It provides quantification of motion with deformation maps between different 4DCT motion states. Because it plays Image registration principles are described in section 1.2.6. The image registration is not included in TRiP4D, so an external software must provide the necessary deformation maps.

The calculation of 4D dose starts with the division of the treatment plan into sub-plans, according to the motion phase it will irradiate. The number of sub-plans is the same as number of motion phases (or number of motion phases in gating window, if gating is used). Afterwards the dose is calculated in each of the motion phases used. Finally, dose in each voxel is then transformed with the deformation maps obtained from registration, in the reference phase to get accumulated dose, see Fig. 1.14. If biological dose is calculated, then instead of the dose, particle number and energy spectra is accumulated, so that the RBE can be calculated according to LEM.

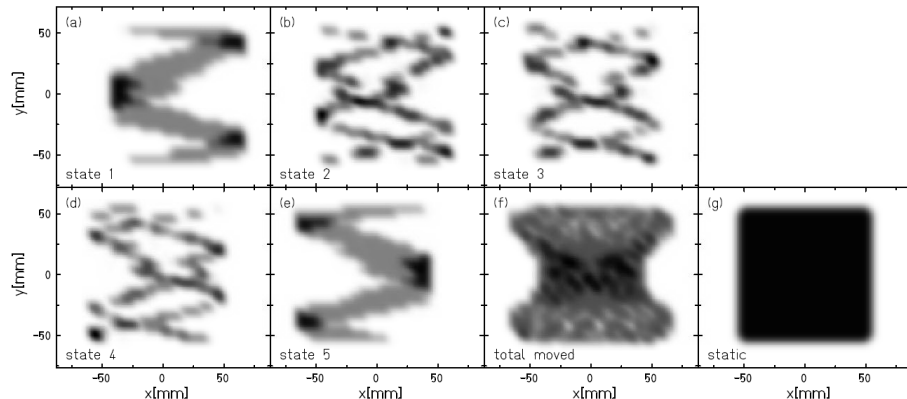


Figure 1.14: Experimental validation of TRiP4D dose calculation on film response. On images a)-e) the individual dose deposition for the five motion state is showed. Image f) shows accumulated 4D dose and image g) a homogeneous dose on a statonary film. Figure taken from [Richter, 2012]

Image registration

Image registration is used to quantitatively assess the temporal changes of the anatomy, as demonstrated in Fig. 1.15. It is used to obtain deformation maps between different motion phases of 4DCT as well as between different consecutive CTs or even between different imaging modalities, e.g. between PET and CT or MRI and CT. There are different possible types of registration and can be placed in two groups. First groups consist of linear registration that include translation, rotation and scaling. The most common used linear transformation used in medical imaging is translation or rigid registration. Other group are elastic or deformable registrations. The actual algorithms for performing registration are complex and reader can find detailed review elswehre [Hill et al., 2001, Brock et al., 2006, Rietzel and Chen, 2006]. A multi-institutional study has shown that the accuracy for the majority of the algorithms is at the order of image voxel size, i.e. milimiters [Brock, 2010]. The study further states that the registration quality depends on image contrast. The quality of image registration is actually hard to quantitatively assess and usually the registration results are checked by eye. To improve image registration quality assurance a special software was developed and is described in detail in chapter **REF**.

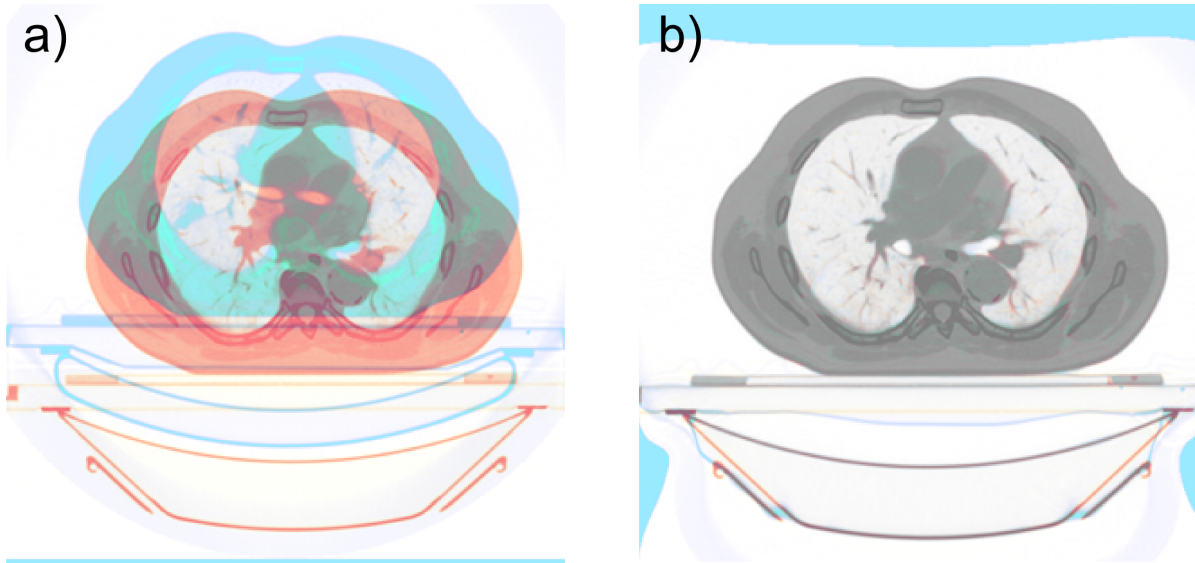


Figure 1.15: Overlap of two CT scans of one patient before (a) and after (b) registration. Inverse colors are used in both CTs so that the overlaid image should be gray where the images overlap perfectly.

1.3 Lung cancer

There were 1.8 million new lung cancer cases diagnosed worldwide in 2012 [Wor,]. With a very poor prognosis (5-year survival rates in Germany is 16% for men and 21% for women [Kaatsch et al., 2014]), lung cancer is one of the most frequent and most deadly cancer types. Usually lung cancer is distinguished into small-cell lung cancer (SCLC) and non-small cell lung cancer (NSCLC). Around 14% of lung cancer cases are SCLC [Tsao,], which is normally treated with chemotherapy and radiotherapy, while for the NSCLC the traditional course of treatment is surgery and radiotherapy.

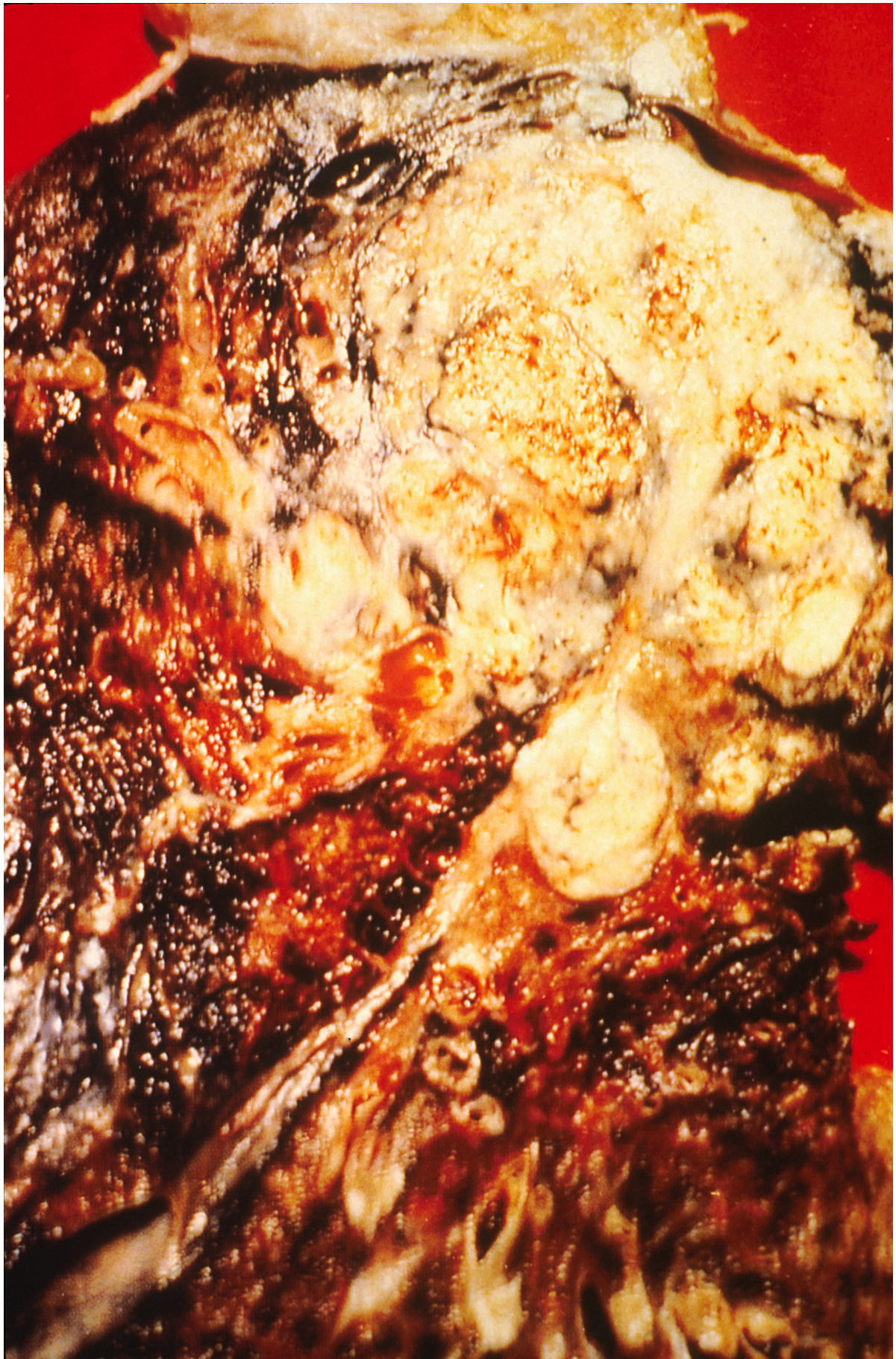


Figure 1.16: Cross section of a human lung. The white area in the upper lobe is cancer, the black areas indicate the patient was a smoker. Figure taken from [NCI, 1988]

1.3.1 Causes

The main cause for lung cancer is a long-term exposure to tobacco smoke [Tsao,], with 85% of cases contributed to smoking. There are over 70 known carcinogens in cigarette smoke, such as benzo[a]pyrene, 1,3-butadiene and a radioactive isotope of polonium, polonium-210 [Hecht, 2012]. Studies have shown that passive smokers have an increased risk of lung cancer as well, with more than 20% increase in risk for those who live with someone who smoke and 16-19% increase for someone working with a smoker [Taylor et al., 2007]. There is some controversy whether smoking cannabis increases risk of lung cancer - two reviews from 2013 and 2014 have found contradicting results [Tashkin, 2013, Underner et al., 2014].

The other 15% of lung cancer cases is attributed to a combination of genetic factors, exposure to radon gas, asbestos or other forms of air pollution [J. and M., 2010].

20-Year Lag Time Between Smoking and Lung Cancer

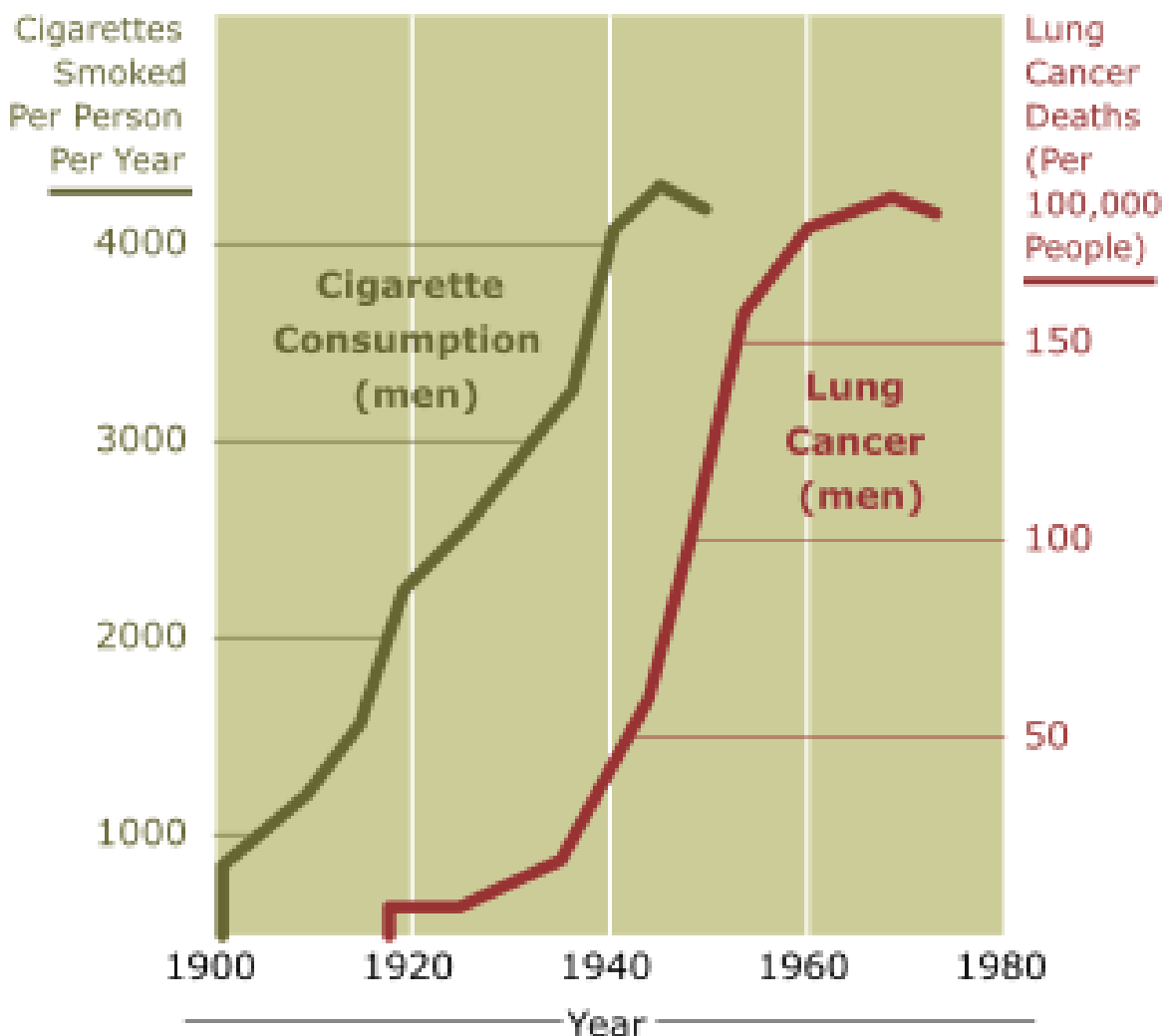


Figure 1.17: Correlation between sales of tobacco products and the rate of the lung cancer in the USA between 1900 - 1970. Data released from National Cancer Institute.

1.3.2 Non-small cell lung cancer

The NSCLC is divided into three main groups: adenocarcinoma, squamous-cell carcinoma and large-cell (undifferentiated) carcinoma [Kasper et al., 2015]. Between 25-35% of all lung cancer cases are adenocarcinoma, squamous-cell carcinoma contributes to around 30% of lung cases and 10-15% are large-cell carcinoma. The SCLC contributes to the rest.

Lung cancer staging is used to assess the degree of spread of the lung cancer and to establish treatment and prognosis [Chheang and Brown, 2013]. For NSCLC TNM classification is used, which depends on size of the primary tumor (T), involvement of the lymph node (N) and distant metastasis (M) [Kasper et al., 2015]. According to TNM class a group is assigned, from stage 0,

IA, IB, IIA, IIB, IIIA, IIIB to IV. A schematic presentation of some stages is shown on Fig. 1.18. Prognosis is highly dependent on stage, as shown in Table 1.1.

Treatment

For NSCLC, the best prognosis is achieved with complete surgical resection of stage IA disease, with up to 70% of investigations confirming NSCLC. The stage is assessed to determine whether the disease is localized and amenable to surgery or if it has spread to the point where it cannot be cured surgically. CT scan and positron emission tomography are used for this determination.^[3] If mediastinal lymph node involvement is suspected, mediastinoscopy may be used to sample the nodes and assist staging.^[88] Blood tests and pulmonary function testing are used to assess whether a person is well enough for surgery.^[15] If pulmonary function tests reveal poor respiratory reserve, surgery may not be possible.^[3]

In most cases of early-stage NSCLC, removal of a lobe of lung (lobectomy) is the surgical treatment of choice. In people who are unfit for a full lobectomy, a smaller sublobar excision (wedge resection) may be performed. However, wedge resection has a higher risk of recurrence than lobectomy.^[89] Radioactive iodine brachytherapy at the margins of wedge excision may reduce the risk of recurrence.^[90] Rarely, removal of a whole lung (pneumonectomy) is performed.^[89] Video-assisted thoracoscopic surgery (VATS) and VATS lobectomy use a minimally invasive approach to lung cancer surgery.^[91] VATS lobectomy is equally effective compared to conventional open lobectomy, with less postoperative illness.^[92]

In SCLC, chemotherapy and/or radiotherapy is typically used.^[93] However the role of surgery in SCLC is being reconsidered. Surgery might improve outcomes when added to chemotherapy and radiation in early stage SCLC.^[94]

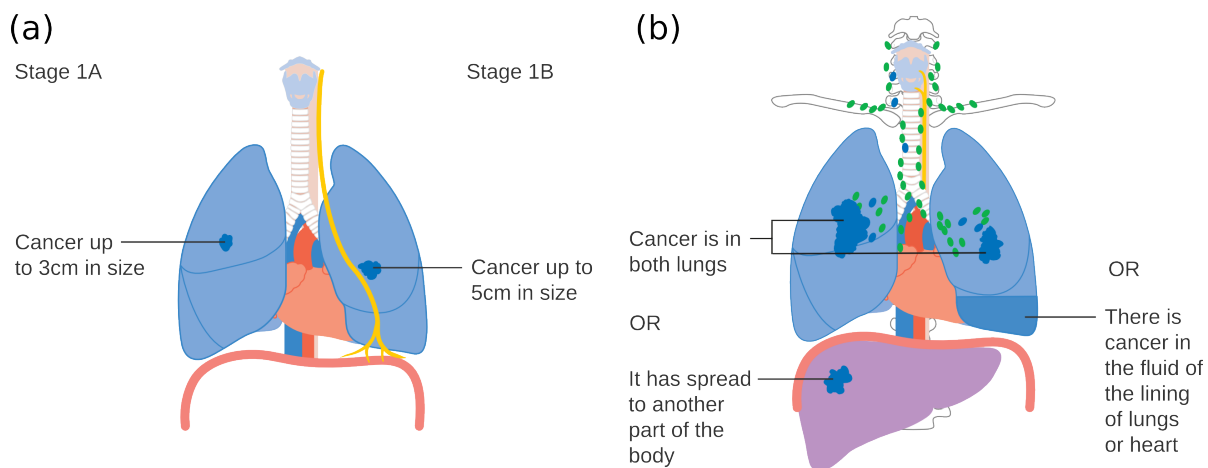


Figure 1.18: Schematic presentation of three NSCLC stages. (a) Stages IA and IB; (b) Stage IV. Figure taken from [CRUK, 2016]

Table 1.1: Five-year survival rates for different stage of NSCLC. Data taken from [Rami-Porta et al., 2009]

Clinical stage	Five-year survival (%)
IA	50
IB	47
IIA	36
IIB	26
IIIA	19
IIIB	7
IV	2



Bibliography

- [Wor,] Worldwide data. <http://www.wcrf.org/int/cancer-facts-figures/worldwide-data>. Accessed: Februar 2016.
- [Ahlen, 1980] Ahlen, S. (1980). Theoretical and experimental aspects of the energy loss of relativistic heavily ionizing particles. *Rev. Mod. Phys.*, 52(1):121.
- [Alpen, 1998] Alpen, E. L. (1998). *Radiation Biophysics*. Academic Press, California, USA, 2nd edition edition.
- [Barkas, 1963] Barkas, H. (1963). *Nuclear Research Emulsions*, volume 1. Academic Press, New York, USA and London, UK.
- [Bert et al., 2008] Bert, C., Groezinger, S. O., and Rietzel, E. (2008). Quantification of interplay effects of scanned particle beams and moving targets. *Phys. Med. Biol.*, 53(9):2253–2265.
- [Bert and Rietzel, 2007] Bert, C. and Rietzel, E. (2007). 4D treatment planning for scanned ion beams. *Radiat. Oncol.*, 2(24).
- [Bethe, 1930] Bethe, H. (1930). Zur Theorie des Durchgangs schneller Korpuskularstrahlung durch Materie. *Annalen der Physik*, 5(5):325–400.
- [Bloch, 1933] Bloch, F. (1933). Zur Bremsung rasch bewegter Teilchen beim Durchgang durch Materie. *Annalen der Physik*, 5(16):285–321.
- [Bohr, 1940] Bohr, N. (1940). Scattering and stopping of fission fragments. *Phys. Rev.*, 58(7):654 – 655.
- [Brock, 2010] Brock, K. K. (2010). Results of a multi-institution deformable registration accuracy study (midras). *Int. J. Radiat. Oncol. Biol. Phys.*, 76(2):583–596.
- [Brock et al., 2006] Brock, K. K., Dawson, L. A., Sharpe, M. B., Moseley, D. J., and Jaffray, D. A. (2006). Feasibility of a novel deformable image registration technique to facilitate classification, targeting and monitoring of tumor and normal tissue. *Int. J. Radiat. Oncol. Biol. Phys.*, 64(4):1245–1254.
- [Brown et al., 2007] Brown, W. T., Wu, X., Fayad, F., Fowler, J. F., Amendola, B. E., Garcia, S., Han, H., de la, Z. A., Bossart, E., Huang, Z., and Schwade, J. G. (2007). Cyberknife radiosurgery for stage I lung cancer: results at 36 months. *Clin. Lung Cancer.*, 8(8):488–492.

- [Chheang and Brown, 2013] Chheang, S. and Brown, K. (2013). Lung cancer staging: Clinical and radiologic perspective. *Semin Intervent Radiol*, 30(2).
- [Chu et al., 1993] Chu, W. T., Ludewigt, B. A., and Renner, T. R. (1993). Instrumentation for treatment of cancer using proton and light-ion beams. *Rev. Sci. Instrum.*, 64(8):2055–2122.
- [CRUK, 2016] CRUK (2016). Cancer research uk (original email from cruk) [cc by-sa 4.0 (<http://creativecommons.org/licenses/by-sa/4.0>)], via wikipedia commons.
- [Elsaesser et al., 2009] Elsaesser, T., Gemmel, A., Scholz, M., Schardt, D., and Krämer, M. (2009). Relevance of very low energy ions for heavy ion therapy. *Phys. Med. Biol.*, 54(7):N101–N106.
- [Elsaesser and Scholz, 2006] Elsaesser, T. and Scholz, M. (2006). Improvement of the local effect model (LEM)—implications of clustered DNA damage. *Radiat. Prot. Dosimetry*, 122(1-4):475–477.
- [Elsaesser and Scholz, 2007] Elsaesser, T. and Scholz, M. (2007). Cluster effects within the local effect model. *Radiat. Res.*, 167(3):319–329.
- [Furukawa et al., 2007] Furukawa, T., Inaniwa, T., Sato, S., Tomitani, T., Minohara, S., Noda, K., and Kanai, T. (2007). Design study of a raster scanning system for moving target irradiation in heavy-ion radiotherapy. *Med. Phys.*, 34(3):1085–1097.
- [Geiss et al., 1999] Geiss, O. B., Schardt, D., Voss, B., Krämer, M., and Kraft, G. (1999). Correlation between CT number and water equivalent thickness. Report.
- [Groezinger, 2004] Groezinger, S. O. (2004). *Volume Conformal Irradiation of Moving Target Volumes with Scanned Ion Beams*. Thesis/dissertation, TU Darmstadt.
- [Haberer et al., 1993] Haberer, T., Becher, W., Schardt, D., and Kraft, G. (1993). Magnetic scanning system for heavy ion therapy. *Nucl. Instrum. Meth. A*, 330:296–305.
- [Hecht, 2012] Hecht, S. S. (2012). Lung carcinogenesis by tobacco smoke. *International Journal of Cancer*, 131(12).
- [Hill et al., 2001] Hill, D. L., Batchelor, P. G., Holden, M., and Hawkes, D. J. (2001). Medical image registration. *Phys. Med. Biol.*, 46(3):R1–45.
- [ICRU, 1993a] ICRU (1993a). Prescribing, recording and reporting photon beam therapy. ICRU report no. 50.
- [ICRU, 1993b] ICRU (1993b). Report 50. Report.
- [ICRU, 1999] ICRU (1999). Prescribing, recording and reporting photon beam therapy, supplement to ICRU report 50. ICRU report no. 62.

[ICRU, 2007] ICRU (2007). ICRU report 78: Prescribing, recording and reporting proton-beam therapy. *Journal of the ICRU*, 7(2).

[J. and M., 2010] J., A. A. and M., S. J. (2010). *Murray & Nadel's Textbook of Respiratory Medicine (5th ed.)*. Saunders Elsevier, Philadelphia, USA.

[Jäkel et al., 2001] Jäkel, O., Jacob, C., Schardt, D., Karger, C. P., and Hartmann, G. H. (2001). Relation between carbon ion ranges and x-ray ct numbers. *Med Phys*, 28:701–703.

[Kaatsch et al., 2014] Kaatsch, P., Spix, C., Hentschel, S., Katalinic, A., Luttmann, S., Stegmaier, C., Caspritz, S., Cernaj, J., Ernst, A., Folkerts, J., Hansmann, J., Kranzhofer, K., Krieghoff-Henning, E., Kunz, B., Penzkofer, A., Treml, K., Wittenberg, K., Baras, N., Barnes, B., Bertz, J., Buttmann-Schweiger, N., Dahm, S., Franke, M., Haberland, J., Kraywinkel, K., Wienecke, A., and Wolf, U. (2014). Cancer in germany 2009/2012. Report.

[Kasper et al., 2015] Kasper, D. L., Hauser, S. L., Jameson, J. L., Fauci, A. S., Longo, D. L., and Loscalzo, J. (2015). *Harrison's Principles of Internal Medicine (19th ed.)*. McGraw-Hill, Columbus, USA.

[Keall et al., 2001] Keall, P. J., Kini, V. R., Vedam, S. S., and Mohan, R. (2001). Motion adaptive x-ray therapy: a feasibility study. *Phys. Med. Biol.*, 46(1):1–10.

[Kiefer and Straaten, 1986] Kiefer, J. and Straaten, H. (1986). A model of ion track structure based on classical collision dynamics. *Phys. Med. Biol.*, 31(11):1201–1209.

[Kilby et al., 2010] Kilby, W., Dooley, J. R., Kuduvali, G., Sayeh, S., and C. R. Maurer, J. (2010). The cyberknife robotic radiosurgery system in 2010. *Technol. Cancer Res. Treat.*, 9(5):433–452.

[Kraft, 2000] Kraft, G. (2000). Tumor therapy with heavy charged particles. *Progress in Particle and Nuclear Physics*, 45(Supplement 2):S473–S544.

[Krämer et al., 2000] Krämer, M., Jäkel, O., Haberer, T., Kraft, G., Schardt, D., and Weber, U. (2000). Treatment planning for heavy-ion radiotherapy: physical beam model and dose optimization. *Phys. Med. Biol.*, 45(11):3299–3317.

[Krämer and Scholz, 2000] Krämer, M. and Scholz, M. (2000). Treatment planning for heavy-ion radiotherapy: calculation and optimization of biologically effective dose. *Phys. Med. Biol.*, 45(11):3319–3330.

[Krämer et al., 2003] Krämer, M., Wang, J. F., and Weyrather, W. (2003). Biological dosimetry of complex ion radiation fields. *Phys. Med. Biol.*, 48(14):2063–2070.

[Langen and Jones, 2001] Langen, K. M. and Jones, D. T. L. (2001). Organ motion and its management. *Int. J. Radiat. Oncol. Biol. Phys.*, 50(1):265–278.

- [Lilley, 2006] Lilley, J. (2006). *Nuclear Physics - Principles and Applications*. Wiley, Manchester, UK.
- [Liu et al., 2007] Liu, H. H., Balter, P., Tutt, T., Choi, B., Zhang, J., Wang, C., Chi, M., Luo, D., Pan, T., Hunjan, S., Starkschall, G., Rosen, I., Prado, K., Liao, Z., Chang, J., Komaki, R., Cox, J. D., Mohan, R., and Dong, L. (2007). Assessing respiration-induced tumor motion and internal target volume using four-dimensional computed tomography for radiotherapy of lung cancer. *Int. J. Radiat. Oncol. Biol. Phys.*, 68(2):531–540.
- [Lu et al., 2006] Lu, H. M., Safai, S., Schneider, R., Adams, J. A., Chen, Y. L., Wolfgang, J. A., Sharp, G. C., Brett, R. C., Kirch, D. G., Hong, T. S., Delaney, T. F., Jiang, S. B., Kooy, H. M., and Chen, G. T. Y. (2006). Respiratory-gated proton therapy treatment. In *Abstract Book PTCOG 44*.
- [Minohara et al., 2000] Minohara, S., Kanai, T., Endo, M., Noda, K., and Kanazawa, M. (2000). Respiratory gated irradiation system for heavy-ion radiotherapy. *Int. J. Radiat. Oncol. Biol. Phys.*, 47(4):1097–1103.
- [Mitaroff et al., 1998] Mitaroff, A., Kraft-Weyrather, W., Geiss, O. B., and Kraft, G. (1998). Biological verification of heavy ion treatment planning. *Radiat. Environ. Biophys.*, 37(1):47–51.
- [Molière, 1948] Molière, G. (1948). Theorie der streuung schneller geladener teilchen ii, mehrfach- und vielfachstreuung. *Zeitschrift für Naturforschung*, 3a:78–97.
- [Munro, 1970] Munro, T. R. (1970). The relative radiosensitivity of the nucleus and cytoplasm of chinese hamster fibroblasts. *Radiat. Res.*, 42(3):451–470.
- [NCI, 1988] NCI (1988). <https://visualsonline.cancer.gov/details.cfm?imageid=2348>.
- [Paganetti et al., 2002] Paganetti, H., Niemierko, A., Ancukiewicz, M., Gerweck, L. E., Goitein, M., Loeffler, J. S., and Suit, H. D. (2002). Relative biological effectiveness (RBE) values for proton beam therapy. *Int. J. Radiat. Oncol. Biol. Phys.*, 53(2):407–421.
- [Phillips et al., 1992] Phillips, M. H., Pedroni, E., Blattmann, H., Boehringer, T., Coray, A., and Scheib, S. (1992). Effects of respiratory motion on dose uniformity with a charged particle scanning method. *Phys. Med. Biol.*, 37(1):223–233.
- [Rami-Porta et al., 2009] Rami-Porta, R., Crowley, J. J., and Goldstraw, P. (2009). The revised tn_m staging system for lung cancer. *Ann Thorac Cardiovasc Surg*, 15(1).
- [Richter, 2012] Richter, D. (2012). *Treatment planning for tumors with residual motion in scanned ion beam therapies*. Thesis/dissertation, TU Darmstadt.

- [Richter et al., 2013] Richter, D., Schwarzkopf, A., Trautmann, J., Kramer, M., Durante, M., Jakel, O., and Bert, C. (2013). Upgrade and benchmarking of a 4d treatment planning system for scanned ion beam therapy. *Medical Physics*, 40(5):051722.
- [Rietzel and Chen, 2006] Rietzel, E. and Chen, G. T. Y. (2006). Deformable registration of 4D computed tomography data. *Med. Phys.*, 33(11):4423–4430.
- [Rietzel et al., 2005] Rietzel, E., Chen, G. T. Y., Choi, N. C., and Willet, C. G. (2005). Four-dimensional image-based treatment planning: Target volume segmentation and dose calculation in the presence of respiratory motion. *Int. J. Radiat. Oncol., Biol., Phys.*, 61(5):1535–1550.
- [Rietzel et al., 2007] Rietzel, E., Schardt, D., and Haberer, T. (2007). Range accuracy in carbon ion treatment planning based on ct-calibration with real tissue samples. *Radiat. Oncol.*, 2(1):14.
- [Saito et al., 2009] Saito, N., Bert, C., Chaudhri, N., Durante, M., Gemmel, A., Lüchtenborg, R., Schardt, D., and Rietzel, E. (2009). Technical status of the real-time beam tracking system. Report.
- [Schardt et al., 2010] Schardt, D., Elsaesser, T., and Schulz-Ertner, D. (2010). Heavy-ion tumor therapy: Physical and radiobiological benefits. *Rev. Mod. Phys.*, 82(1):383.
- [Scholz and Kraft, 1994] Scholz, M. and Kraft, G. (1994). Calculation of heavy ion inactivation probabilities based on track structure, x ray sensitivity and target size. *Radiat. Prot. Dosim.*, 52(1–4):29–33.
- [Sonke et al., 2008] Sonke, J. J., Lebesque, J., and van, H. M. (2008). Variability of four-dimensional computed tomography patient models. *Int. J. Radiat. Oncol. Biol. Phys.*, 70(2):590–598.
- [Tashkin, 2013] Tashkin, D. P. (2013). Effects of marijuana smoking on the lung. *Annals of the American Thoracic Society*, 10(3).
- [Taylor et al., 2007] Taylor, R., F., N., and A., D. (2007). Meta-analysis of studies of passive smoking and lung cancer: effects of study type and continent. 36(5).
- [Tsao,] Tsao, A. S. Lung carcinoma. Merck Manual Professional Edition. Accessed: Februar 2016.
- [Underner et al., 2014] Underner, M., Urban, T., and Perriot, J. (2014). Cannabis smoking and lung cancer. *Revue des Maladies Respiratoires*, 31(6).

- [van de Water et al., 2009] van de Water, S., Kreuger, R., Zenklusen, S., Hug, E., and Lomax, A. J. (2009). Tumour tracking with scanned proton beams: assessing the accuracy and practicalities. *Phys. Med. Biol.*, 54(21):6549–6563.
- [Varma et al., 1977] Varma, M. N., Baum, J. W., and Kuehner, A. V. (1977). Radial dose, LET and W for 160 ions in N₂ and tissue-equivalent gases. *Radiat. Res.*, 70(3):511–518.
- [Zenklusen et al., 2010] Zenklusen, S. M., Pedroni, E., and Meer, D. (2010). A study on re-painting strategies for treating moderately moving targets with proton pencil beam scanning at the new gantry 2 at PSI. *Phys. Med. Biol.*, 55(17):5103–5121.